Electronic Supplementary Information (ESI)

Reduced graphene oxide supported Ni nanoparticles: A high performance reusable heterogeneous catalyst for Kumada–Corriu cross-coupling reactions

Koushik Bhowmik,[a,‡] Debasish Sengupta,[b,‡] Basudeb Basu [b,*] and Goutam De [a,*]

[a]Nano-Structured Materials Division, CSIR–Central Glass and Ceramic Research Institute, 196, Raja S. C. Mullick Road, Kolkata 700032 (India)

[b]Department of Chemistry, North Bengal University, Darjeeling-734013, India

E–mail: gde@gcri.res.in, basu_nbu@hotmail.com

S1. Control experiments using Ni/RGO-20, Ni/RGO-60 and bare Ni NP.

Ni/RGO-20 and Ni/RGO-60 were synthesized following the method mentioned in section 2.3. Both the materials were characterized by XRD and the results are shown in Fig. S2. Both samples show characteristic peaks of Ni(111), Ni(200) and RGO similar to those of Ni/RGO-40 (see Fig. 3a). However, as expected, the relative XRD peak intensities of metallic Ni and RGO are different in the three samples due to the variation of compositions. The crystallite size of Ni in the three Ni/RGO samples were evaluated using the X-ray line broadening method (Scherrer's equation) from Fig. S2 and Fig. 3a. In case of Ni, the crystallite size was evaluated from both the (111) and (200) peaks. Following this method we found the average crystallite size of Ni as 10, 12 and 17 nm in Ni/RGO-20, Ni/RGO-40 and Ni/RGO-60 samples, respectively. TEM of Ni/RGO-40 confirms existence of Ni NPs of average size ~11 nm. As mentioned above the relative peak intensity of RGO is highest in case of Ni/RGO-20 and lowest for Ni/RGO-60.

Control reactions were performed to establish the better performance of Ni/RGO-40 composite following the similar reaction conditions as mentioned in the experimental section (see section 2.4). For this purpose Ni/RGO-60, Ni/RGO-20 and bare Ni NPs were used as catalysts. The amount of different

catalysts was used in such a way that the concentration of Ni (0.1 mmol with respect to 1 mmol of 4–iodoanisole) remained constant in all cases. The results are summarized in Table S1. It can be seen that Ni/RGO-40 showed the highest catalytic activity.

The deterioration of catalytic activity of Ni/RGO-60 (Table S1; entry 2) can be understood because of larger size of Ni NPs (17 nm) with lower active surfaces. This is expected because chances of agglomeration of Ni would be higher due to high amount of Ni loading. Although we found little lowering of Ni NPs' size (10 nm) in case of Ni/RGO-20, the yield of the reaction was found to be dropped in this case also (Table S1; entry 3) when compared with Ni/RGO-40 (Table S1; entry 1). In case of Ni/RGO-20, we believe that the exposed Ni surface got reduced due to the presence of more RGO.

The bare Ni NPs of size around 10 nm was also tested as catalyst (Table S1; entry 4) under similar reaction conditions which produces only 63% yield. The control reaction without any catalyst showed 8% yield (Table S1; entry 5) and the yield can be increased to 14% if the reaction continued up to 24 h (Table S1; entry 6). Therefore from the above results, it can be concluded that Ni/RGO-40 is an optimized composition for the Kumada–Corriu cross-coupling reactions.

Table S1 Control reactions to compare the catalytic activity of Ni/RGO-40[a]

Entry	Solvent	Catalyst	Ni content [with respect to 4-iodo-anisole (mmol)]	Temperature(°C)	Time (h)	Yield (%)[b]
1	THF	Ni/RGO-40	0.1	25	4	89
2	THF	Ni/RGO-60	0.1	25	4	67
3	THF	Ni/RGO-20	0.1	25	4	77
4	THF	Ni NPs	0.1	25	4	63
5	THF	Nil	00	25	4	08
6	THF	Nil	00	25	24	14

[a] 4–Iodoanisole (1 mmol), PhMgCl (1 mL, 25 wt% in THF, 1.84 mmol), solvent (2 mL), under N_2, [b] Isolated yield

S2. The melting point and the characteristic feature of ^1H and ^{13}C NMR spectra of coupled products.

4-Methoxybiphenyl[1] (Fig. S3.1; Table 2, entry 1, 8, 9)

White solid, m.p. 90-91 ^oC (Literature: 91-92 ^oC); ^1H NMR ($CDCl_3$, 300 MHz): δ/ppm 3.84 (s, 3H, OCH_3), 6.97 (dd, J = 6.9 and 2.1 Hz, 2H, ArH), 7.29-7.32 (m, 1H, ArH), 7.38-7.43 (m, 2H,

ArH), 7.51-7.56 (m, 4H, ArH); ^{13}C NMR ($CDCl_3$, 75 MHz): δ/ppm 55.3, 114.2, 126.6, 126.7, 128.1, 128.7, 133.8, 140.8, 159.2.

3-Methoxybiphenyl[2] **(**Fig. S3.2; Table 2, entry 2, 5**)**

Colorless liquid; ^{1}H NMR ($CDCl_3$, 300 MHz): δ/ppm 3.86 (s, 3H, OCH_3), 6.90 (ddd, J = 8.1 Hz, 2.4 Hz and 0.9 Hz, 1H, ArH), 7.12-7.13 (m, 1H, ArH), 7.16-7.20 (m, 1H, ArH), 7.33-7.38 (m, 2H, ArH), 7.41-7.46 (m, 2H, ArH), 7.57-7.60 (m, 2H, ArH); ^{13}C NMR ($CDCl_3$, 75 MHz):δ/ppm 55.3, 112.7, 112.9, 119.7, 127.2, 127.4, 128.7, 129.7, 141.1, 142.8, 159.9.

2-Methoxybiphenyl[3] **(**Fig. S3.3; Table 2, entry 3**)**

Colorless liquid; ^{1}H NMR ($CDCl_3$, 300 MHz): δ/ppm 3.81 (s, 3H, OCH_3), 6.97-7.06 (m, 2H, ArH), 7.29-7.43 (m, 5H, ArH), 7.51-7.54 (m, 2H, ArH); ^{13}C NMR ($CDCl_3$, 75 MHz): δ/ppm 55.5, 111.2, 120.8, 126.9, 127.9, 128.6, 129.5, 130.7, 130.9, 138.5, 156.4.

4-Methoxy-4'-methylbiphenyl[4] (Fig. S3.4; Table 2, entry 4)

White solid, m.p. 112-113 ^{o}C (Literature: 111-112 ^{o}C); ^{1}H

NMR ($CDCl_3$, 300 MHz): δ/ppm 2.38 (s, 3H, CH_3), 3.84 (s, 3H, OCH_3), 6.96 (d, J = 8.7 Hz, 2H, ArH), 7.22 (d, J = 8.4 Hz, 2H, ArH), 7.45 (d, J = 8.1 Hz, 2H, ArH), 7.51 (d, J = 8.7 Hz, 2H, ArH); ^{13}C NMR ($CDCl_3$, 75 MHz): δ/ppm 21.0, 55.3, 114.1,

126.5, 127.9, 129.4, 133.7, 136.3, 137.9, 158.9.

3-Methoxy-3'-methylbiphenyl[2] (Fig. S3.5; Table 2, entry 6)

colorless liquid; ^{1}H NMR ($CDCl_3$, 300 MHz): δ/ppm 2.41 (s, 3H, CH_3), 3.84 (s, 3H, OCH_3), 6.87-6.89 (m, 1H, ArH), 7.11-8.18 (m, 3H, ArH), 7.28-7.39 (m, 4H, ArH); ^{13}C NMR ($CDCl_3$, 75 MHz): δ/ppm 21.5, 55.2, 112.6, 112.8, 119.6, 124.3, 127.9, 128.1, 128.6, 129.6, 138.3, 141.0, 142.8, 159.8.

4-Methoxy-3-methylbiphenyl[5] (Fig. S3.6; Table 2, entry 7)

White solid, m.p. 75-76 ^{o}C (Literature: 74-75 ^{o}C); ^{1}H NMR ($CDCl_3$, 300 MHz): δ/ppm 2.28 (s, 3H, CH_3), 3.87 (s, 3H, OCH_3), 6.89 (d, J = 9.3 Hz, 1H, ArH), 7.25-7.31 (m, 1H, ArH), 7.38-7.43 (m, 4H, ArH), 7.53-7.56 (m, 2H, ArH); ^{13}C NMR ($CDCl_3$, 75 MHz): δ/ppm 16.4, 55.4, 110.1, 125.3, 126.5, 126.7, 126.9, 128.6, 129.5, 133.3, 141.0, 157.3.

***m*-Terphenyl**[6] (Fig. S3.7; Table 2, entry 10, 11, 12)

White solid, m.p. 83-85 ^{o}C (Literature: 84-85 ^{o}C); ^{1}H NMR ($CDCl_3$, 300 MHz): δ/ppm 7.33-7.38 (m, 2H, ArH), 7.43-7.59 (m, 7H, ArH), 7.63-7.66 (m, 4H, ArH), 7.79-7.80 (m, 1H, ArH); ^{13}C NMR ($CDCl_3$, 75 MHz): δ/ppm 126.1, 126.2, 127.3, 127.4, 128.8, 129.2, 141.2, 141.8.

***o*-Terphenyl**[5] (Fig. S3.8; Table 2, entry 13, 14)

White solid, m.p. 54-55 ^{o}C (Literature: 54-56 ^{o}C); ^{1}H NMR ($CDCl_3$, 300 MHz): δ/ppm 7.13-7.26 (m, 10H, ArH), 7.40-7.44 (m, 4H, ArH); ^{13}C NMR ($CDCl_3$, 75 MHz): δ/ppm 126.4, 127.4, 127.8, 129.9, 130.6, 140.6, 141.5.

4,4′-Dimethoxybiphenyl[7] (Fig. S3.9; Table 2, entry 15)

White crystalline solid, m.p. 179-180 ^{o}C (Literature: 178-179 ^{o}C); ^{1}H NMR ($CDCl_3$, 300 MHz): δ/ppm 3.84 (s, 6H, OCH_3), 6.96 (d, J = 9 Hz, 4H, ArH), 7.48 (d, J = 8.7 Hz, 4H, ArH); ^{13}C NMR ($CDCl_3$, 75 MHz): δ/ppm 55.3, 114.1, 127.7, 133.4, 158.6.

2-Phenylpyridine[8] (Fig. S3.10; Table 2, entry 17)

Colorless liquid; ^{1}H NMR ($CDCl_3$, 300 MHz): δ/ppm 7.18-7.26 (m, 1H, ArH), 7.39-7.51 (m, 3H, ArH), 7.72-7.80 (m, 2H, ArH), 7.96-8.00 (m, 2H, ArH), 8.70 (d, J = 4.5 Hz, 1H, ArH); ^{13}C NMR ($CDCl_3$, 75 MHz): δ/ppm 115.4, 120.7, 122.1, 127.0, 128.7, 129.0, 129.6, 136.8, 139.3, 149.6, 157.5.

References:

(1) E. Alacid and C. Najera, *Org. Lett*., 2008, **10**, 5011−5014.

(2) B. Basu, K. Biswas, S. Kundu and S. Ghosh, *Green Chem*., 2010, **12**, 1734−1738.

(3) S. D. Jackson, J. Wills, G. J. Kelly, G. D. McLellan, G. Webb, S. Mather, R. B. Moyes, S. Simpson, P. B. Wells and R. Whymen, *Phys. Chem. Chem. Phys.*, 1999, **1**, 2573−2580.

(4) L. Wang and Z. X. Wang, *Org. Lett*., 2007, **9**, 4335−4338.

(5) B. Basu, S. Das, P. Das, B. Mandal, D. Banerjee and F. Almqvist, *Synthesis*, **2009**, 1137−1146.

(6) X. H. Fan and L. M. Yang, *Eur. J. Org. Chem.*, 2011, 1467–1471.

(7) G. Cahiez, C. Chaboche, F. Mahuteau-Betzer and M. Ahr, *Org. Lett*., 2005, **7**, 1943−1946.

(8) D. Srimani and A. Sarkar, *Tetrahedron Lett*., 2008, **49**, 6304–6307.

Fig. S1. A comparison of the ^{13}C peaks of sp^2-C attached to iodide (in 4-iodoanisole) and that of 4-methoxybiphenyl clearly exhibit complete conversion through Kumada–Corriu C–C cross-coupling reaction.

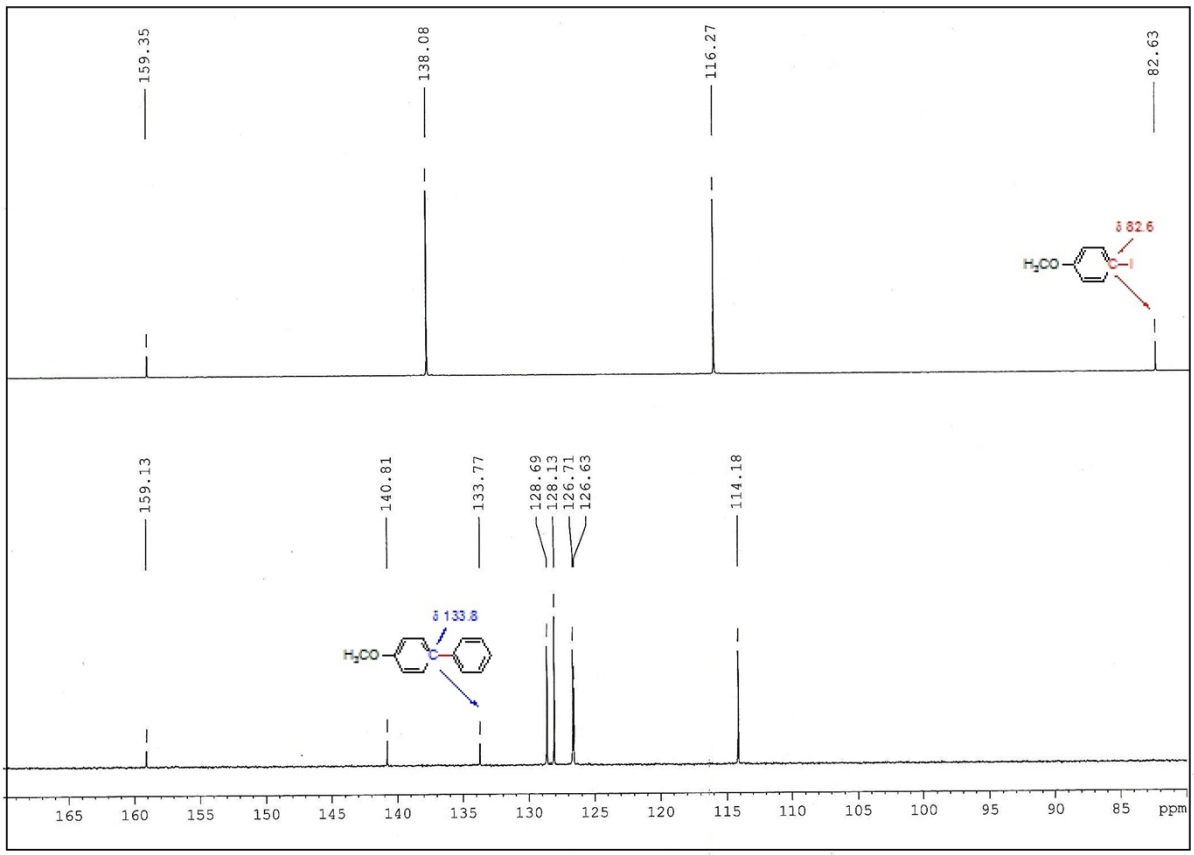

Fig. S2 XRD patterns of Ni/RGO-20 (a) and Ni/RGO-60 (b)

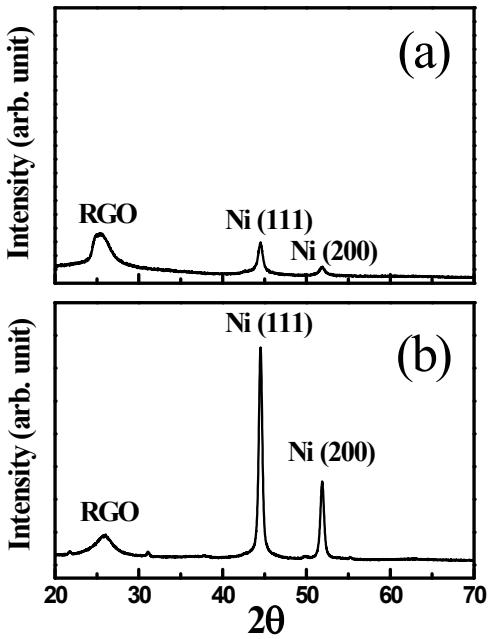

Fig. S3. Scanned ^{1}H and ^{13}C NMR spectra of cross-coupling products.
Fig. S3.1 Table 2, entry 1, 8, 9

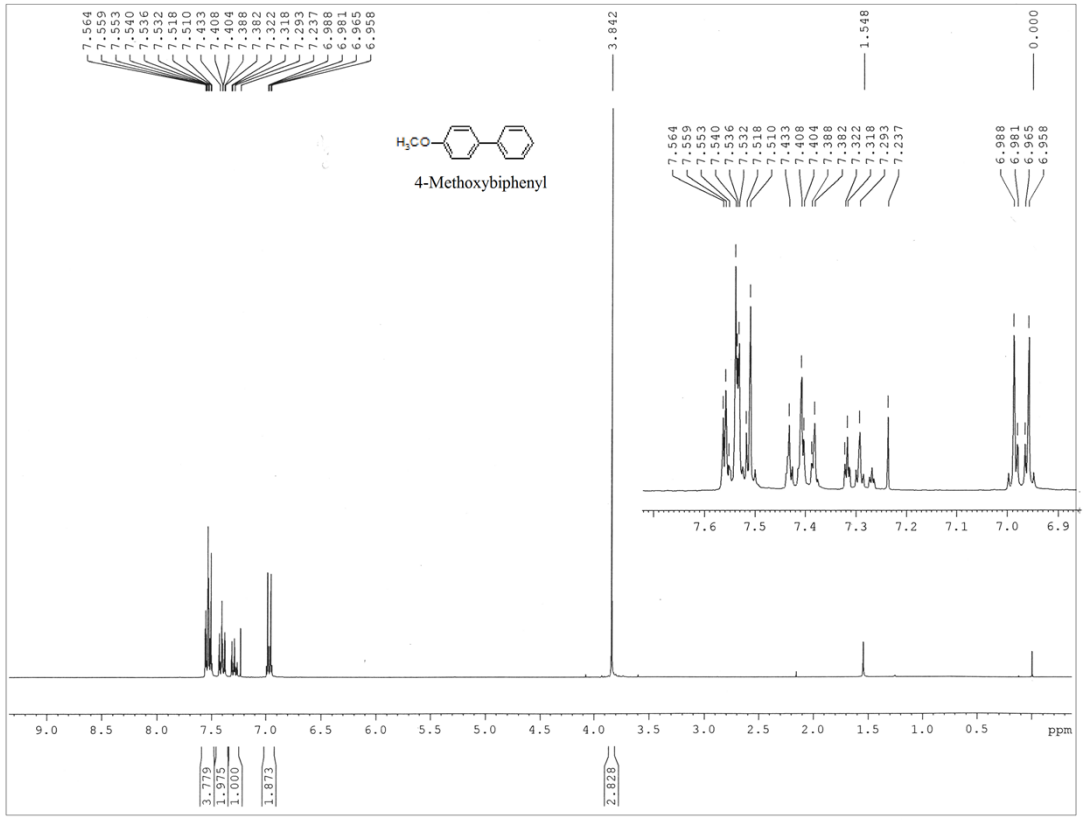

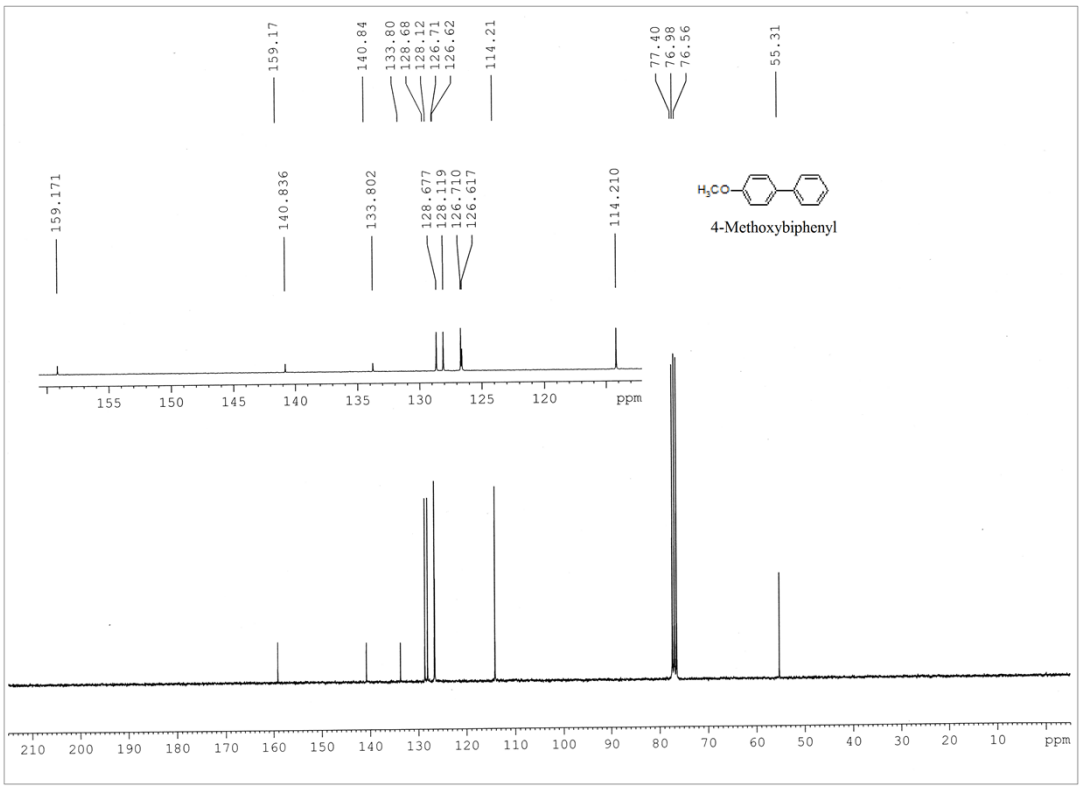

Fig. S3.2 Table 2, entry 2, 5

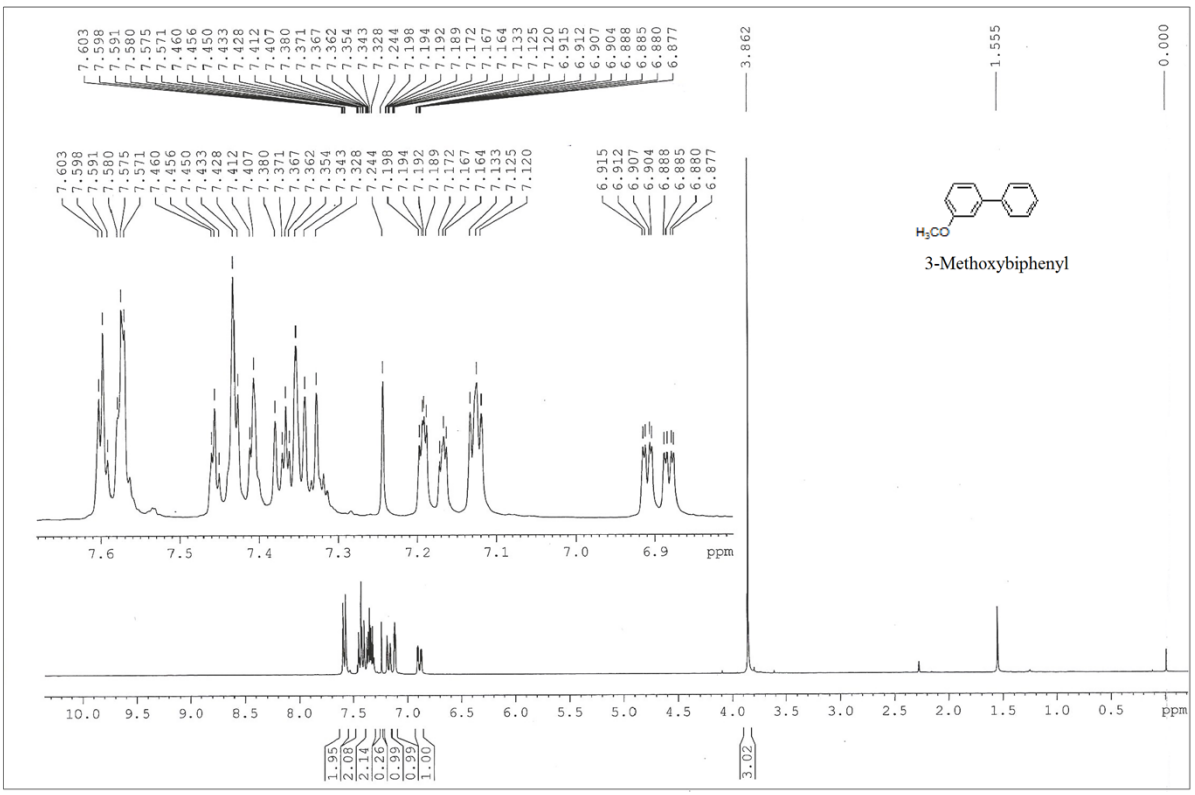

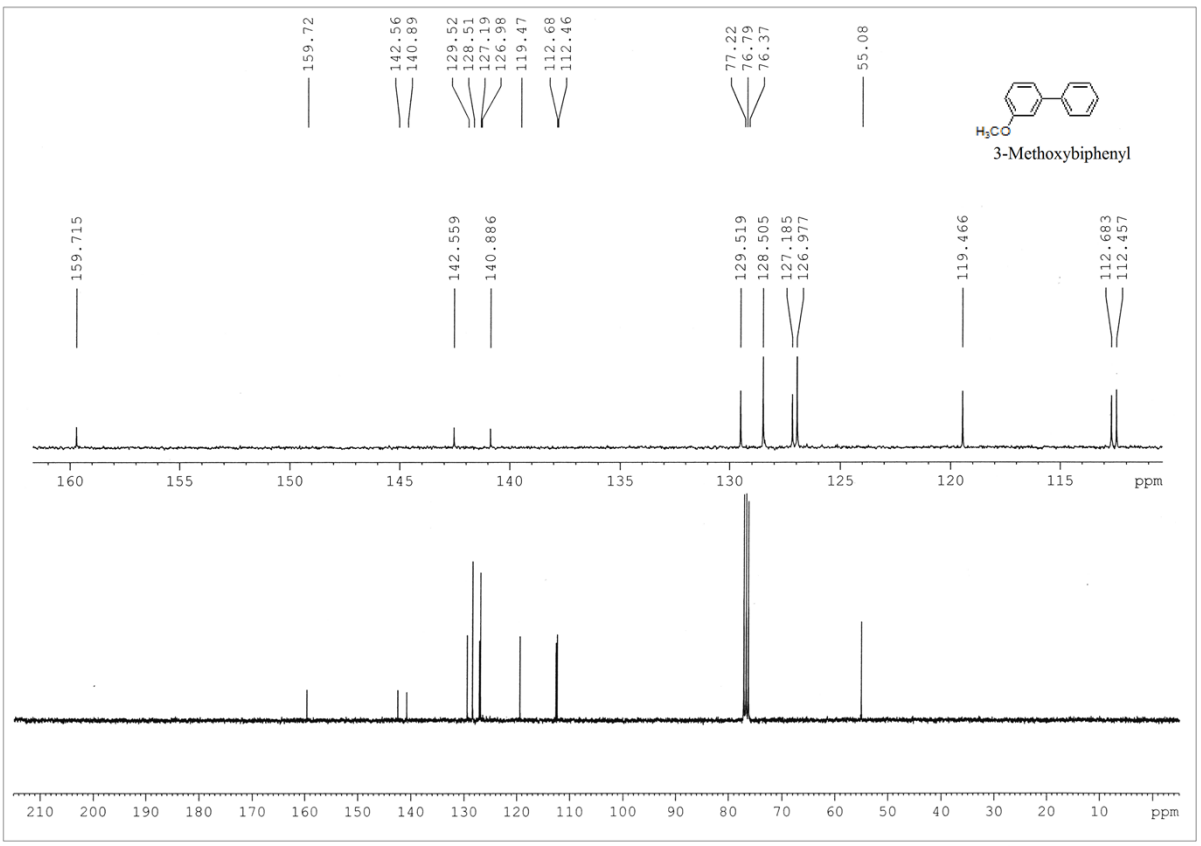

Fig. S3.3 Table 2, entry 3

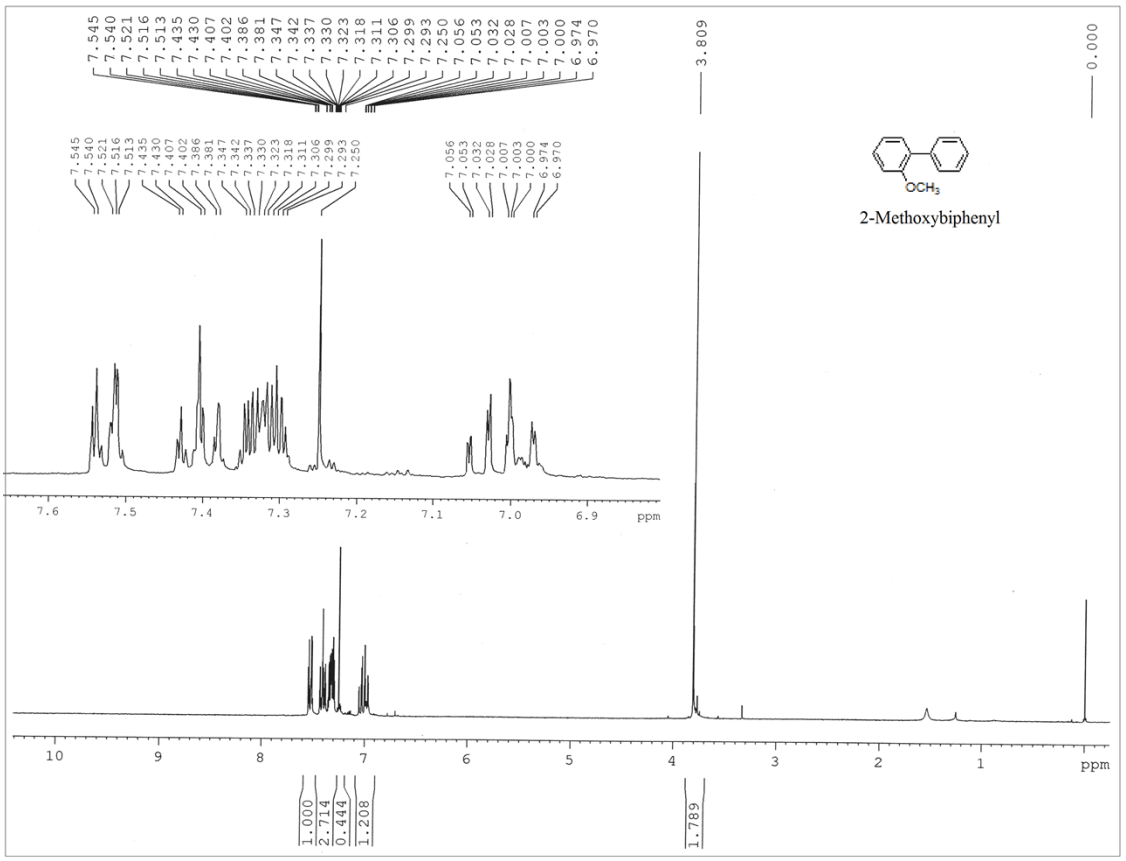

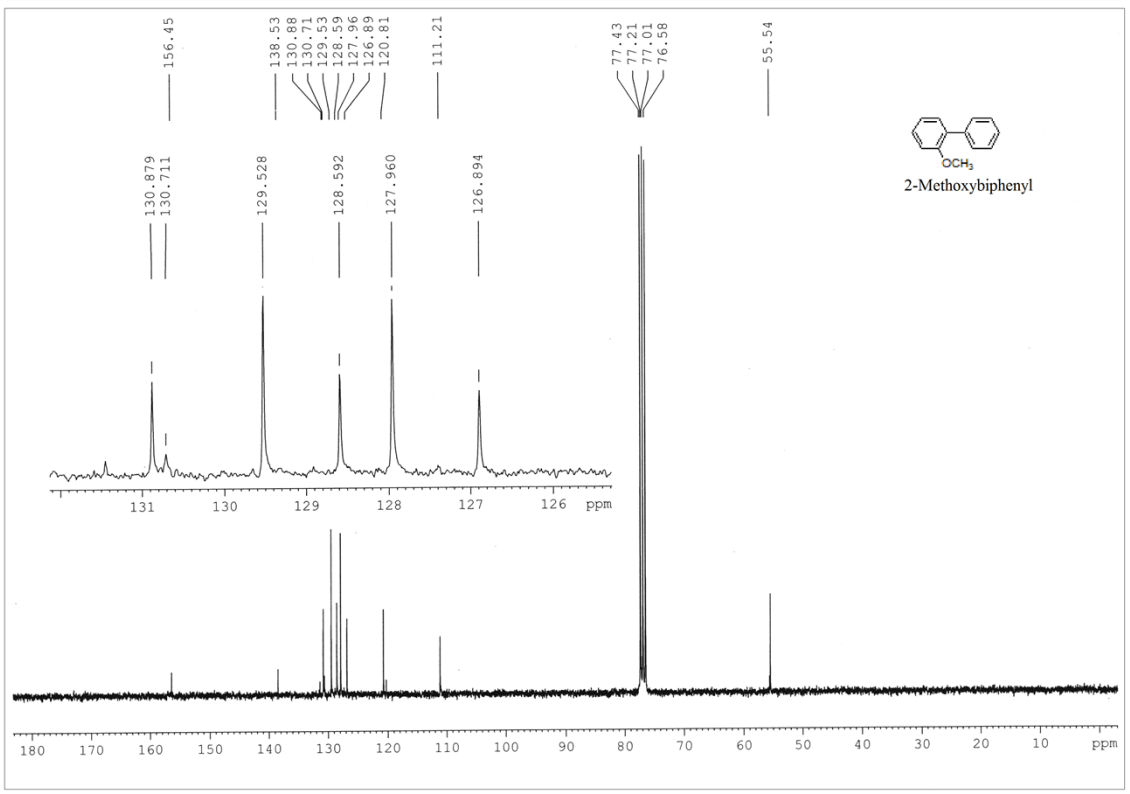

Fig. S3.4 Table 2, entry 4

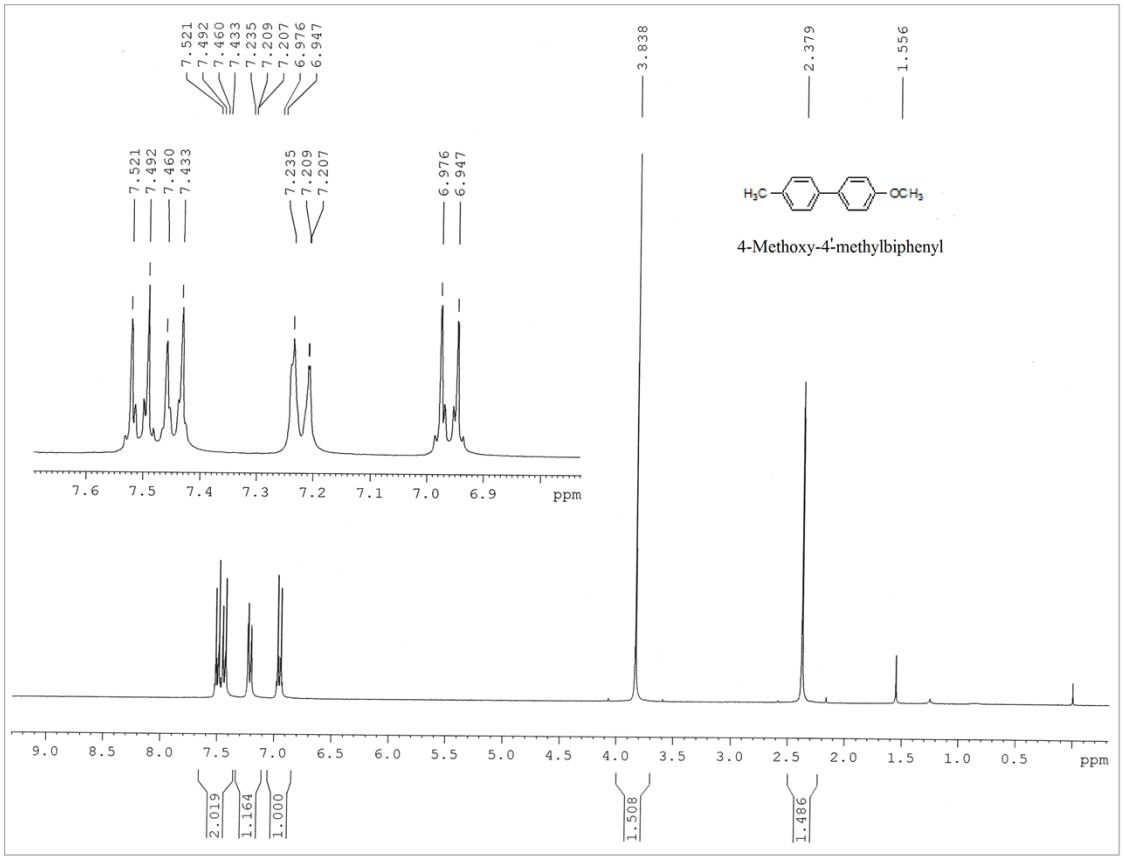

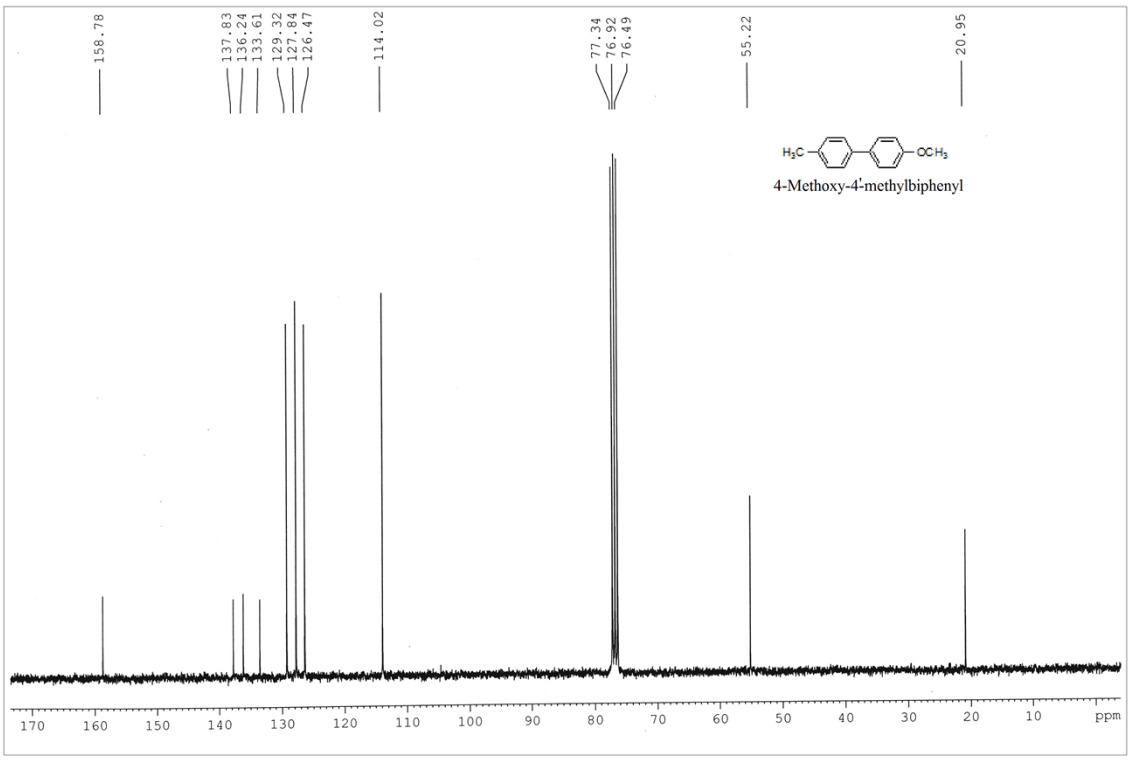

Fig. S3.5 Table 2, entry 6

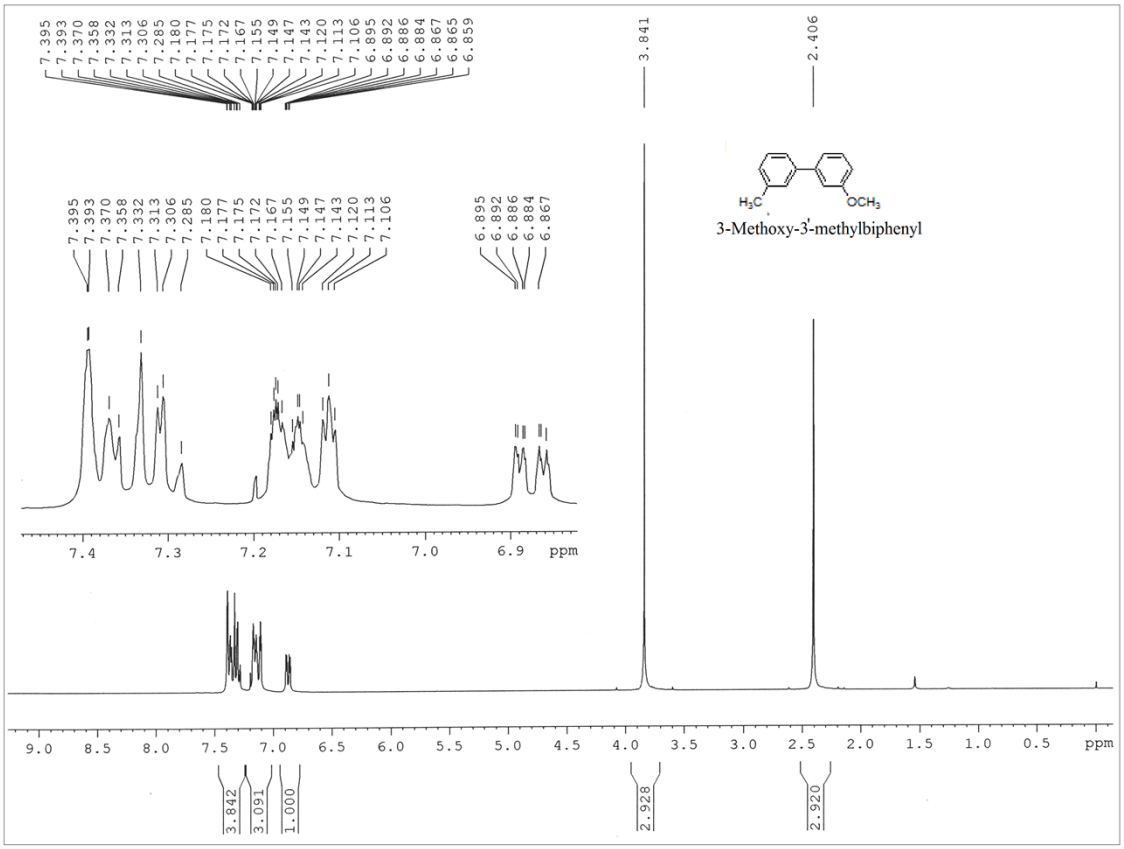

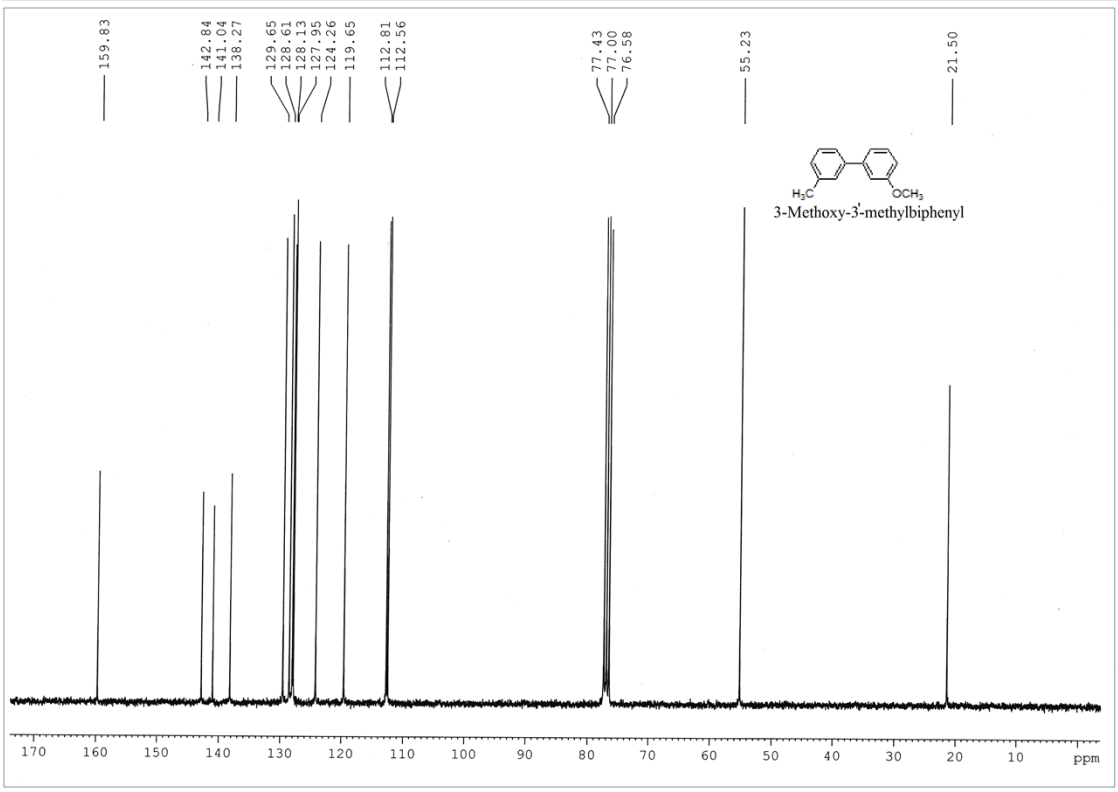

Fig. S3.6 Table 2, entry 7

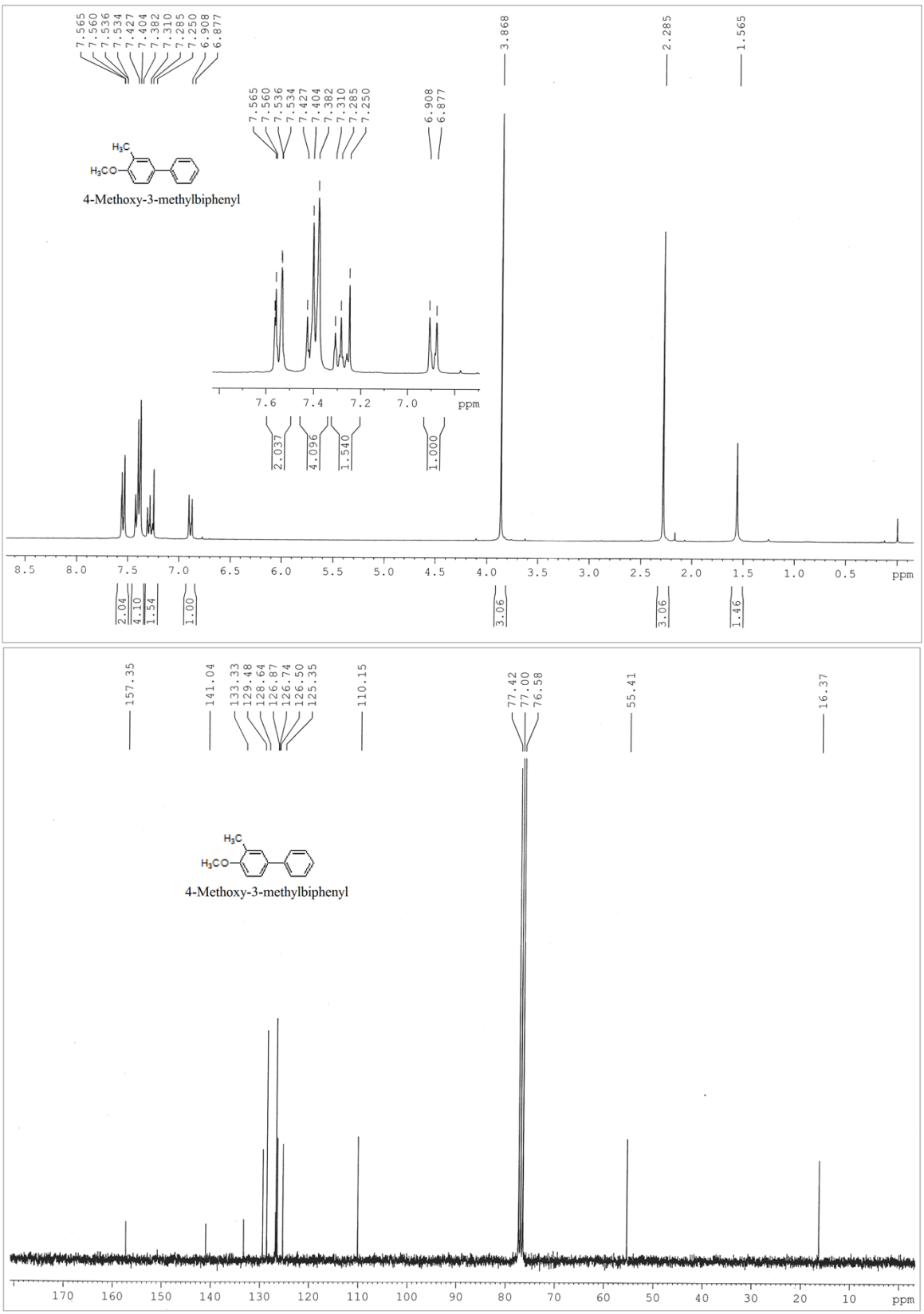

Fig. S3.7 Table 2, entry 10, 11, 12

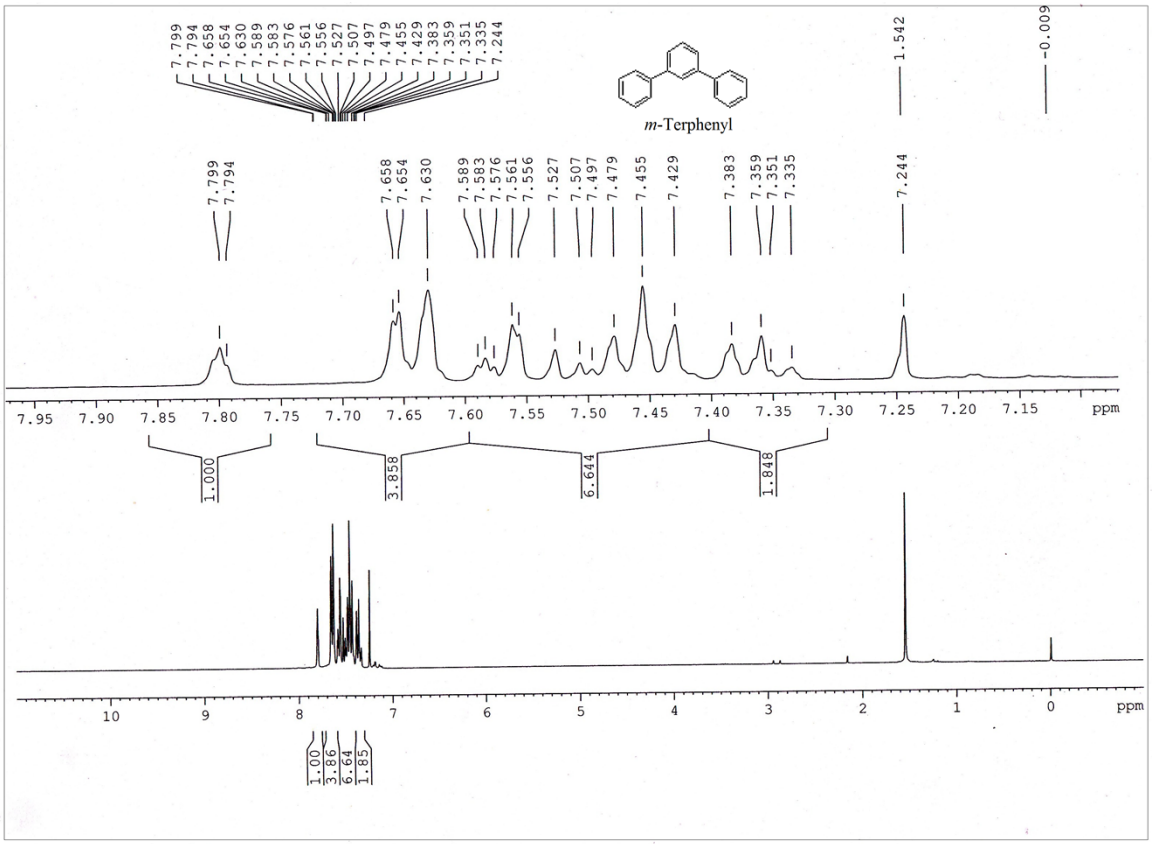

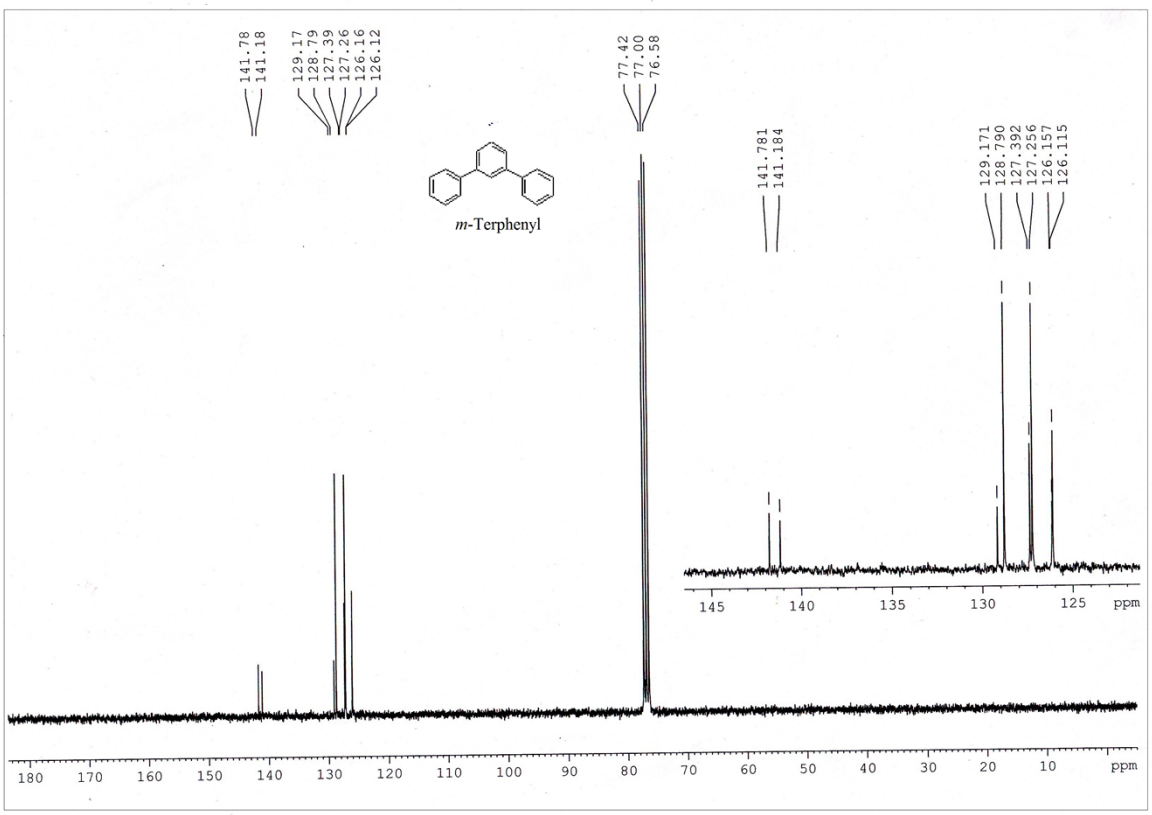

Fig. S3.8 Table 2, entry 13, 14

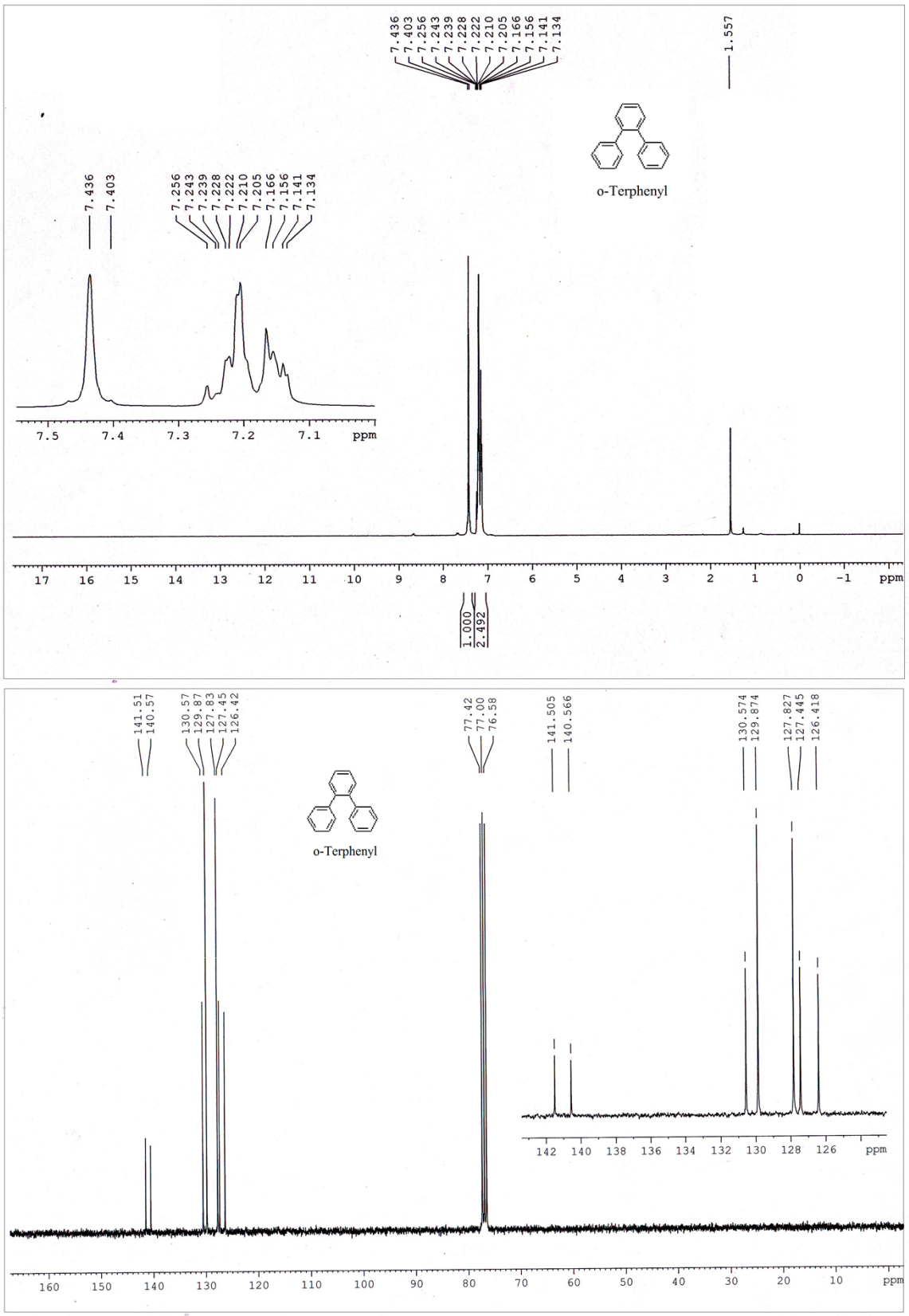

Fig. S3.9 Table 2, entry 15

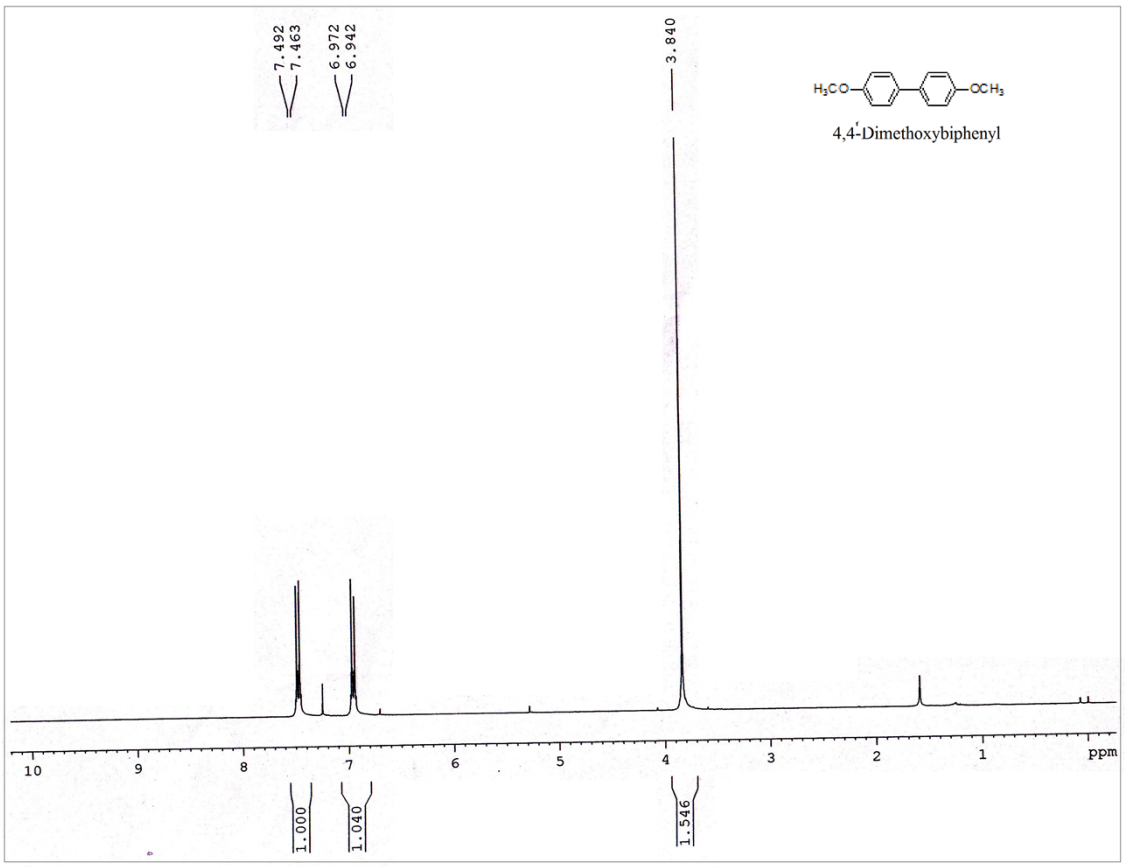

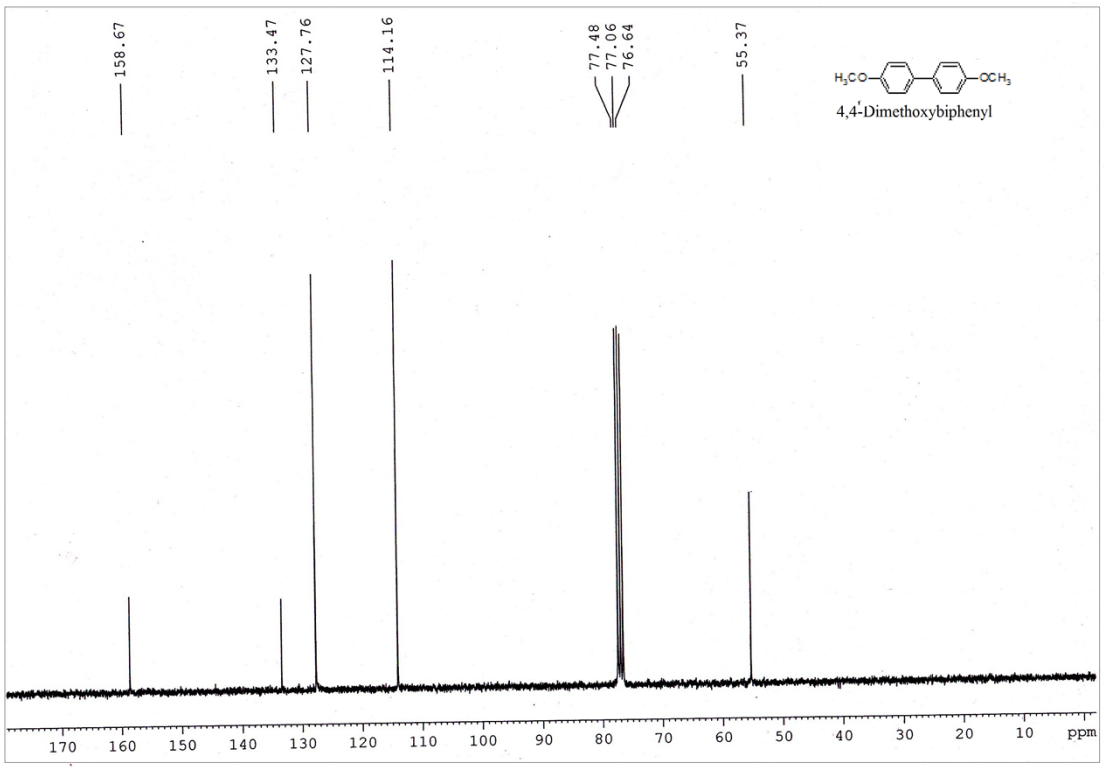

Fig. S3.10 Table 2, entry 17

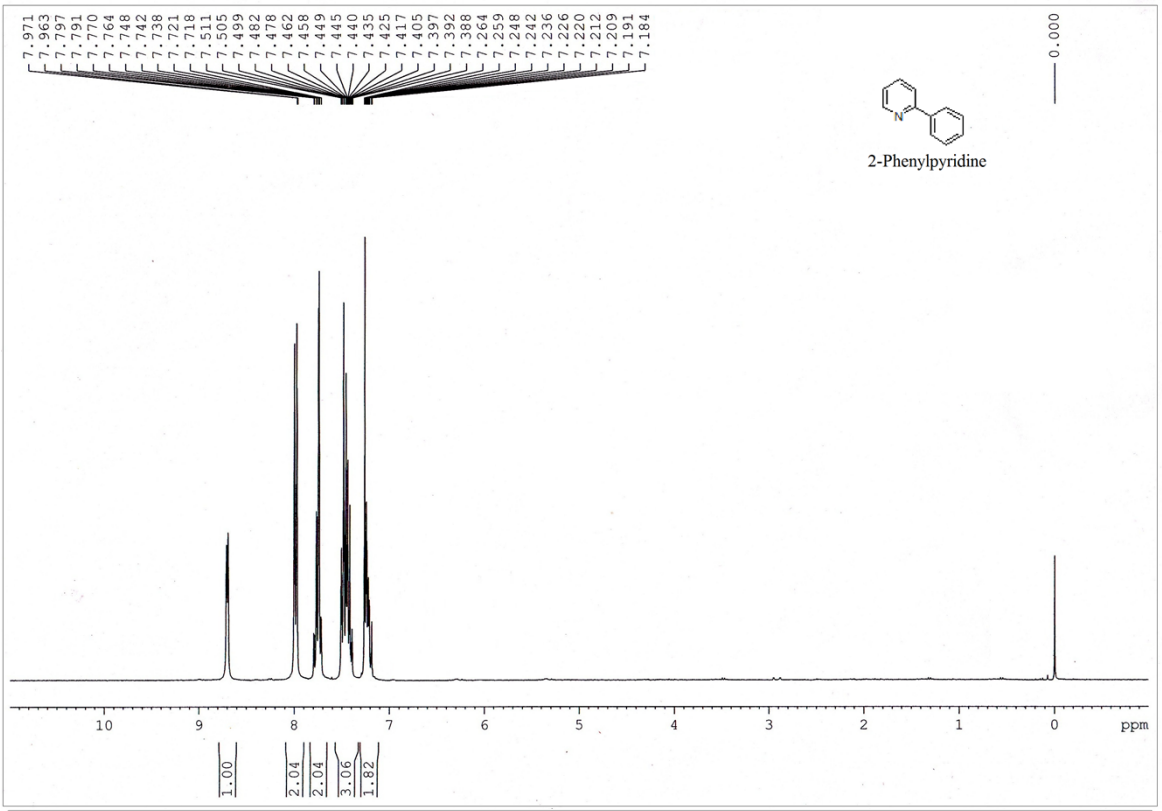

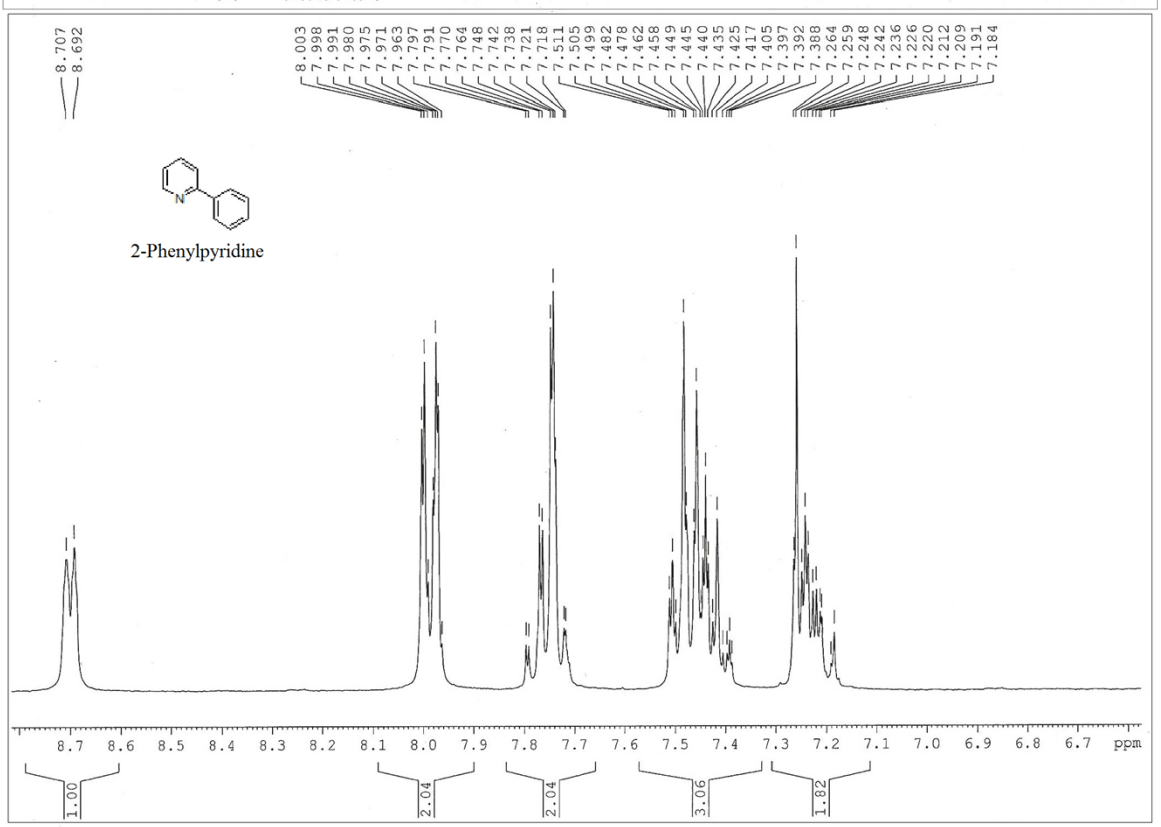

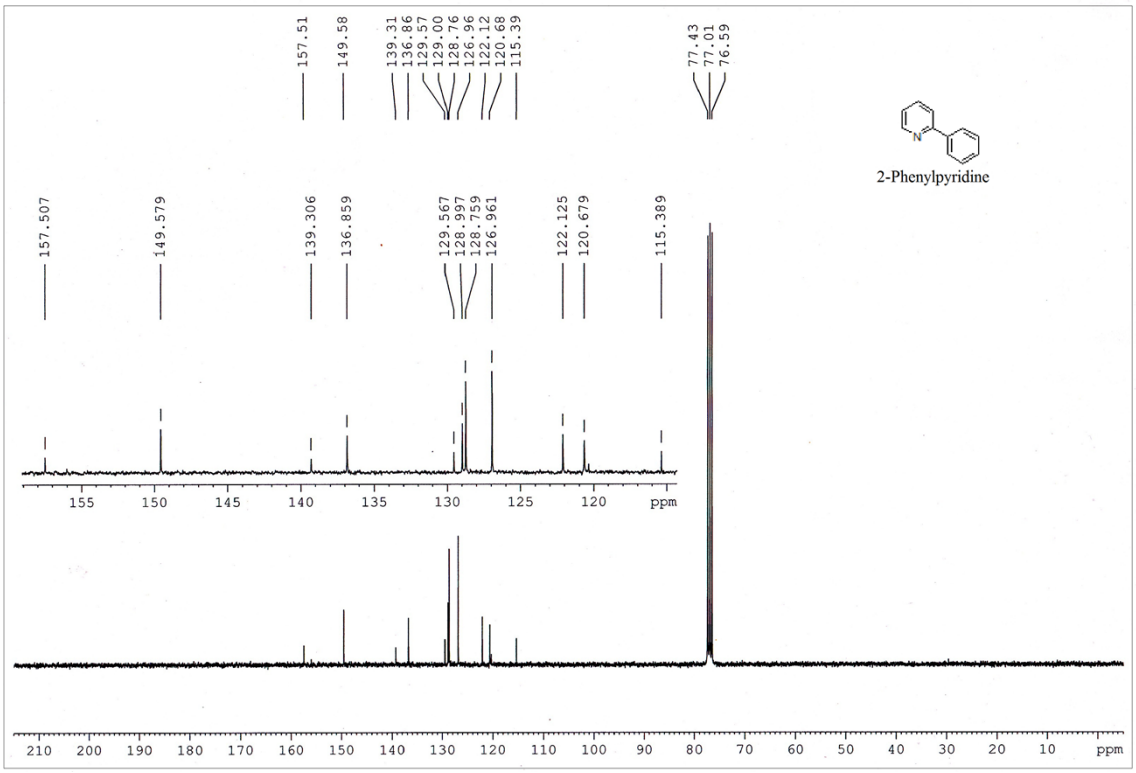
157.51
149.58
139.31
136.86
129.57
129.00
128.76
126.96
122.12
120.68
115.39
77.43
77.01
76.59
2-Phenylpyridine
157.507
149.579
139.306
136.859
129.567
128.997
128.759
126.961
122.125
120.679
115.389
155 150 145 140 135 130 125 120 ppm
210 200 190 180 170 160 150 140 130 120 110 100 90 80 70 60 50 40 30 20 10 ppm

Fig. S4. XRD of recovered catalyst Ni/RGO-40 after sixth cycle.

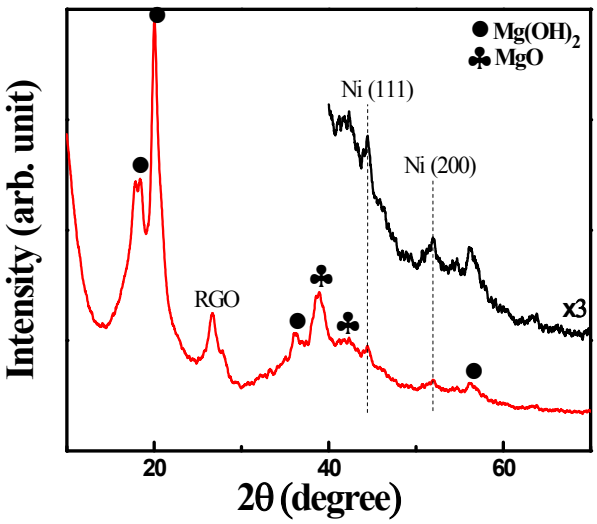

Fig. S5. Raman spectrum of RGO.

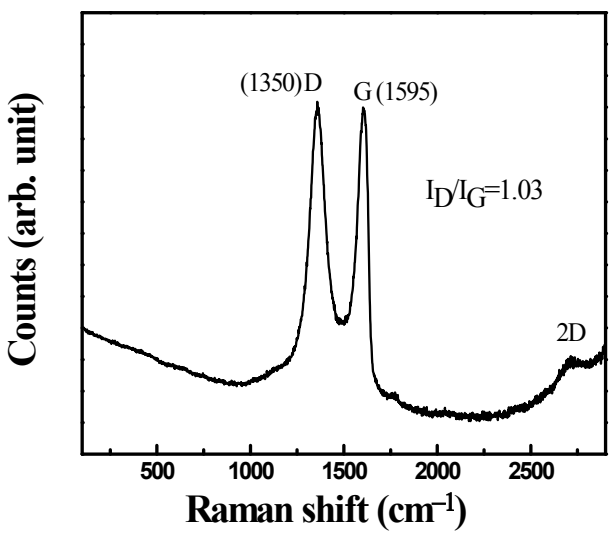

Fig. S6. Raman spectrum of recovered Ni/RGO-40 catalyst after sixth cycle.